PHOTONICS Research

3D waveguide device for few-mode multi-core fiber optical communications

Juncheng Fang,[1,†] Jingbo Hu,[1,†] Yanan Zhong,[1] Aru Kong,[1] Jianxin Ren,[2] Shibiao Wei,[1] Zhenwei Xie,[1] [iD] Ting Lei,[1] Bo Liu,[2,3] and Xiaocong Yuan[1,*]

[1]Nanophotonics Research Centre, Shenzhen Key Laboratory of Micro-Scale Optical Information Technology & Institute of Microscale Optoelectronics, Shenzhen University, Shenzhen 518060, China
[2]Institute of Optoelectronics, Nanjing University of Information Science & Technology, Nanjing 210044, China
[3]e-mail: bo@nuist.edu.cn
*Corresponding author: xcyuan@szu.edu.cn

Space-division multiplexing based on few-mode multi-core fiber (FM-MCF) technology is expected to break the Shannon limit of a single-mode fiber. However, an FM-MCF is compact, and it is difficult to couple the beam to each fiber core. 3D waveguide devices have the advantages of low insertion loss and low cross talk in separating various spatial paths of multi-core fibers. Designing a 3D waveguide device for an FM-MCF requires considering not only higher-order modes transmission, but also waveguide bending. We propose and demonstrate a 3D waveguide device fabricated by femtosecond laser direct writing for various spatial path separations in an FM-MCF. The 3D waveguide device couples the LP01 and LP11a modes to the FM-MCF with an insertion loss below 3 dB and cross talk between waveguides below −36 dB. To test the performance of the 3D waveguide device, we demonstrate four-channel multiplexing communication with two LP modes and two cores in a 1-km few-mode seven-core fiber. The bit error rate curves show that the different degrees of bending of the waveguides result in a difference of approximately 1 dB in the power penalty. Femtosecond laser direct writing fabrication enables 3D waveguide devices to support high-order LP modes transmission and further improves FM-MCF communication.   © 2022 Chinese Laser Press

https://doi.org/10.1364/PRJ.465174

1. INTRODUCTION

With the rapid development of network traffic, existing single-mode fiber communication technology has approached the nonlinear Shannon limit of 100 Tbit/s [1]. Space-division multiplexing (SDM) with multi-core fibers (MCFs) [2,3] and few-mode fibers (FMFs) [4,5] is one of the most promising approaches to breaking the capacity limit. SDM increases fiber capacity using a spatial channel as an additional multiplexing degree of freedom [6–8]. MCF contains multiple single-mode fiber cores, each of which represents an independent information channel. FMF uses orthogonal modes of different orders such as linearly polarized (LP) [9,10], orbital angular momentum [11–13], and cylindrical vector beam modes [14,15] as independent channels to increase fiber capacity. Optical geometric transformation [15–18] and multi-plane light conversion (MPLC) [19–22] provide efficient mode multiplexing/demultiplexing for communication. Currently, single-mode MCFs with more than 30 cores have been demonstrated [23], and FMF transmission with more than 10 modes has been used to increase fiber capacity [24,25]. However, the diameter of MCF is between 125 and 318 μm, and the different cores need

to be kept distant from each other to limit inter-core cross talk, thus limiting the number of cores in the MCF [26]. Moreover, the number of modes used in FMF transmission is limited by the effective refractive index difference between a fiber core and its surroundings [27]. To further increase the fiber capacity, focus has recently turned to combining the MCF and FMF into a few-mode multi-core fiber (FM-MCF) [28]. SDM communication systems with more than 100 spatial channels have been demonstrated in FM-MCFs with data rates exceeding 10 Pb/s [29,30]. While FM-MCFs promise to significantly increase fiber capacity, eventual deployment of FM-MCF networks still requires practical methods to couple individual modes into closely spaced fiber cores.

Besides optical fibers, fan-outs or other means of combining and separating the various spatial paths are needed for SDM based on FM-MCFs. In recent years, several coupling methods have been proposed for FM-MCFs, such as free space coupling [31], photonic wire bonding [32], fused tapers [33], and 3D waveguide devices [34–36]. Photonic integrated devices show great potential in optical fiber communication [37], sensing [38], imaging [39,40], and quantum information systems

[41], especially in combining and separating dense FM-MCF cores [42]. For an SDM system that includes an FM-MCF, a photonic integrated device is indispensable to realizing the optical interconnection between the FMF and FM-MCF. The 3D waveguide device is a photonic integrated device fabricated by femtosecond laser direct writing [43,44] that provides a low insertion loss, low cross talk, and small-size solution for an FM-MCF. The 3D waveguide device consists of multiple waveguides, each of which corresponds to one of the cores of the FM-MCF. Multiple waveguides are spatially bent to separate the closely spaced FM-MCF cores and couple the LP modes into these cores. Propagation of higher-order modes in the waveguide requires a larger effective refractive index difference between the waveguide and the cladding to confine the beam. Therefore, the performance of an FM-MCF communication system based on a 3D waveguide is related to the number of supported modes in the waveguide, the insertion loss between the waveguide and the fiber, and the cross talk between different waveguides.

In this paper, we propose and demonstrate a 3D waveguide device for FM-MCF optical communications. The device is fabricated by laser direct writing. Each waveguide supports LP01, LP11a, and LP11b modes transmission at a wavelength of 1550 nm, and has a diameter of 16.5 μm and an effective refractive index difference larger than 0.0026 with the surrounding material. One side of the 3D waveguide device is a one-dimensional waveguide array composed of seven waveguides with a pitch of 127 μm, and the other side is a seven-core distribution matched to a few-mode seven-core fiber. An MPLC system outputs multiple groups of LP01, LP11a, and LP11b modes that are transmitted in a 3D waveguide device, and the cross talk between different waveguides is less than −36 dB. Then, the 3D waveguide device couples multiple groups of LP01, LP11a, and LP11b modes to the FM-MCF with an insertion loss less than 3 dB, and the cross talk between different FM-MCF cores is less than −30 dB. In the communication experiments, we demonstrate four-channel FM-MCF multiplexing communication consisting of two LP modes and any two of the FM-MCF cores. Measured bit error rates (BERs) show that bending of the waveguide to different degrees causes about a 1-dB difference in power penalty. The 3D waveguide device has application potential in next-generation ultra-capacity FM-MCF optical communication.

2. 3D WAVEGUIDE DESIGN AND FABRICATION

Figure 1 shows the schematic of the 3D waveguide device for FM-MCF coupling. One side of the device is a one-dimensional array of seven waveguides with a pitch of 127 μm for interconnection with the few-mode fiber array [Fig. 1(a)]. The one-dimensional waveguide array is gradually bent in a 3D waveguide device to converge to the central waveguide. Figure 1(b) shows the waveguide array convergence. Viewed from the side of the 3D wave device, multiple waveguides will converge, as shown in Fig. 1(c). Figure 1(d) shows the other side of the 3D waveguide device is a seven-core waveguide structure with six waveguides surrounding the central waveguide with a radius of 42 μm and a spacing of 60°, matching the few-mode seven-core fiber. The waveguide array is bent between the two sides of the 3D waveguide device. After sizing the 3D waveguide device, we optimized the waveguide bending curve to reduce mode leakage, cross talk, and transmission loss, and to determine the device selection. The detailed theory of the S-bend design for 3D waveguide performance optimization was well explained by the literature previously [45,46]. The bending of the waveguide is optimized with the function

$$\begin{cases} y = \frac{6h\sin\theta}{L^5}x^5 - \frac{15h\sin\theta}{L^4}x^4 + \frac{10h\sin\theta}{L^3}x^3 \\ z = \frac{6h\cos\theta}{L^5}x^5 - \frac{15h\cos\theta}{L^4}x^4 + \frac{10h\cos\theta}{L^3}x^3 \end{cases}, \quad \textbf{(1)}$$

where L is the waveguide length, h is the waveguide height, and θ is the angle between h and the z axis. The bending is determined by θ, and an increase in length or a decrease in height will reduce the bending. Numerical simulation shows the refractive index difference of the waveguide is between 0.0018
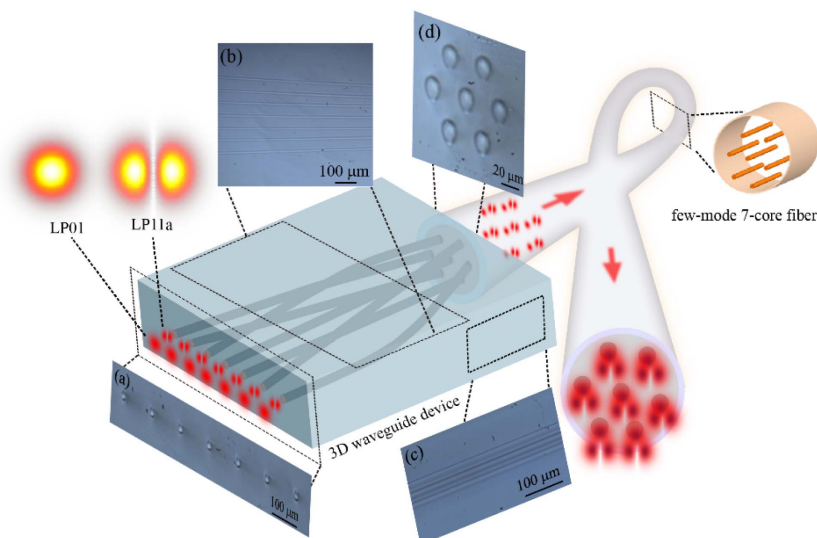

Fig. 1. 3D waveguide device and few-mode seven-core fiber. (a) One side of the 3D waveguide device is a waveguide array. (b) Top view of the 3D waveguide device. (c) Side view of the 3D waveguide device. (d) The other side of the 3D waveguide device is a seven-core arrangement.

and 0.0045, which supports LP01, LP11a, and LP11b modes transmission. Then, we calculated the effect of different effective refractive index differences on the waveguide transmission efficiency for a fixed degree of waveguide bending. Figure 2(a) shows that the transmission efficiency of the LP11a mode or LP11b mode is close to 1 and stable when the waveguide length is 17 mm and the effective refractive index difference is larger than 0.0026. The results show that the transmission efficiency of high-order LP modes is more stable when the fabricated 3D waveguide device has a larger effective refractive index difference. For an effective refractive index difference of 0.0026, we observed the transmission efficiency under different bending curvatures by controlling the length of the 3D waveguide device. Figure 2(b) shows that the transmission efficiency of the LP11a or LP11b mode is stable when the length of the 3D waveguide device is larger than 16 mm. Therefore, the length of the device we fabricated is 17 mm.

The simulation of the LP11a mode considers the bending of the waveguide, and the light spot distribution at different positions in the waveguide is observed by the established bending waveguide model. Figures 2(c) and 2(d) show numerically simulated LP01 and LP11a modes propagating in a 3D waveguide device with each waveguide marked. We calculated the cross talk between different waveguides when the length of the 3D waveguide device is 17 mm and the effective refractive index difference is 0.004. The numerical simulation shows that the cross talk between different waveguides is less than

−50 dB, which is almost negligible. We also calculated the transmission loss efficiencies of LP01 and LP11a modes in different waveguides, as shown in Table 1. Compared with those in other channels, the waveguides of channels 1 and 7 have the greatest bending curvatures and the lowest transmission efficiencies.

Femtosecond lasers have the advantages of ultra-short pulse duration and high peak intensity, providing a solution for 3D waveguide device fabrication. The 3D waveguide devices in our experiments were fabricated by femtosecond laser direct writing. The setup of the femtosecond laser direct writing is shown in Appendix A. When a femtosecond laser is focused on the fabricated substrate, the refractive index of the focal region changes permanently owing to the rapid absorption of laser energy via nonlinear mechanisms. The area where the femtosecond laser is focused has a refractive index difference with the material of the surrounding substrate, which is used for the light beam transmission. The design of the 3D waveguide device was optimized by adjusting various parameters such as rep-

Table 1. Calculated Transmission Efficiencies of LP01 and LP11a in Different Waveguides

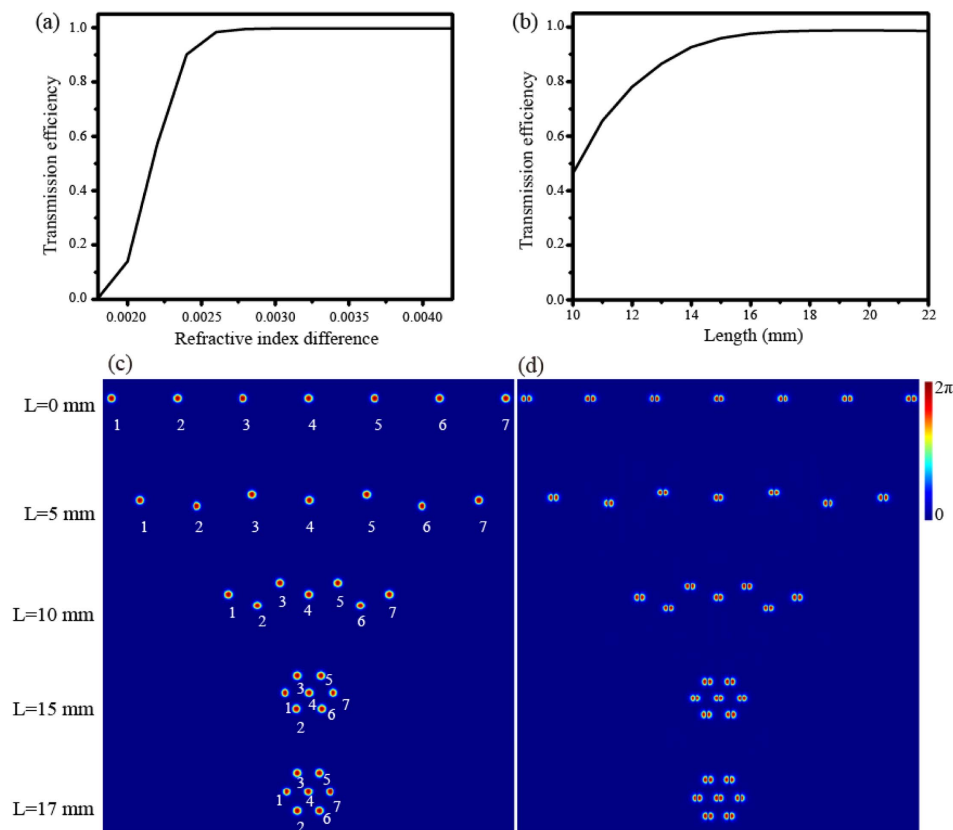| Channel	1	2	3	4	5	6	7
LP01	0.9990	0.9991	0.9991	0.9999	0.9991	0.9991	0.9990
P11a	0.9968	0.9980	0.9986	0.9998	0.9986	0.9980	0.9968

Fig. 2. Numerically simulated effect of (a) different effective refractive index differences for a 3D waveguide length of 17 mm and (b) bending curvature on the waveguide transmission efficiency when the effective refractive index difference is 0.0026. Numerically simulated (c) LP01 mode and (d) LP11a mode distributions at different positions in the 3D waveguide device.

etition rate, pulse width, material properties, and depth of focus. We then chose a femtosecond laser with a wavelength of 1030 nm, pulse width of 180 fs, single pulse energy of 200 nJ, and repetition rate of 200 kHz. The 3D waveguide device was fabricated by focusing a femtosecond laser at 150 μm below the glass surface with a 40× objective. The device has a refractive index difference larger than 0.0026 and supports LP01, LP11a, and LP11b modes transmission. The waveguide sizes are matched to FMFs to reduce insertion loss, resulting in a designed waveguide diameter of 16.5 μm. Higher-order LP modes transmission can be obtained by increasing the effective refractive index difference between the waveguide and the surrounding material, which requires improved waveguide fabrication techniques.

3. EXPERIMENTAL RESULTS AND ANALYSIS

In the experiments, multiple LP modes were generated by MPLC and coupled to one side of the 3D waveguide device by a one-dimensional few-mode fiber array. The multiple LP modes were output from the other side of the 3D waveguide device, as shown in Figs. 3(a) and 3(b). In the experiments, the LP modes of the seven cores are generated by seven individual MPLC LP mode multiplexers [21]. The MPLC has coaxial output of LP modes in few-mode fiber as the input modes coupling to the waveguides. Any perturbation or bending of the

fiber will cause the LP11a mode rotation. Therefore, the input and the output LP11a modes have various rational deviations from the horizontal direction. Figure 3(c) shows the few-mode seven-core fiber (the few-mode seven-core fiber supports six LP mode transmissions, as shown in Appendix B). The distribution of the light beam output from the 3D waveguide device is consistent with the core distribution of the few-mode seven-core fiber. We then coupled the light beam output of the 3D waveguide device to a few-mode seven-core fiber using the experimental setup in Fig. 3(d). Figures 3(e) and 3(f) show the LP01 and LP11a modes output from the 1-km few-mode seven-core fiber. The insertion losses of the LP01 and LP11a modes from the few-mode fiber array to the few-mode seven-core fiber are less than 1.7 dB and 2.7 dB, respectively, including the insertion losses from the few-mode fiber to the 3D waveguide device and the 3D waveguide device to the few-mode seven-core fiber. Numerical simulations show that the insertion loss of the LP01 mode is increased by 0.3 dB and that of the LP11a mode by 1 dB owing to the mismatch in refractive index distributions of the waveguide and the fiber. Figure 3(g) shows the insertion losses of LP01 and LP11a modes coupled to seven cores. In addition, the return loss of the fiber-waveguide is measured as less than −25 dB by using an optical circulator. The insertion loss can be reduced by optimizing the waveguide size and refractive index distribution to improve the match to the fiber core. The insertion loss of LP01
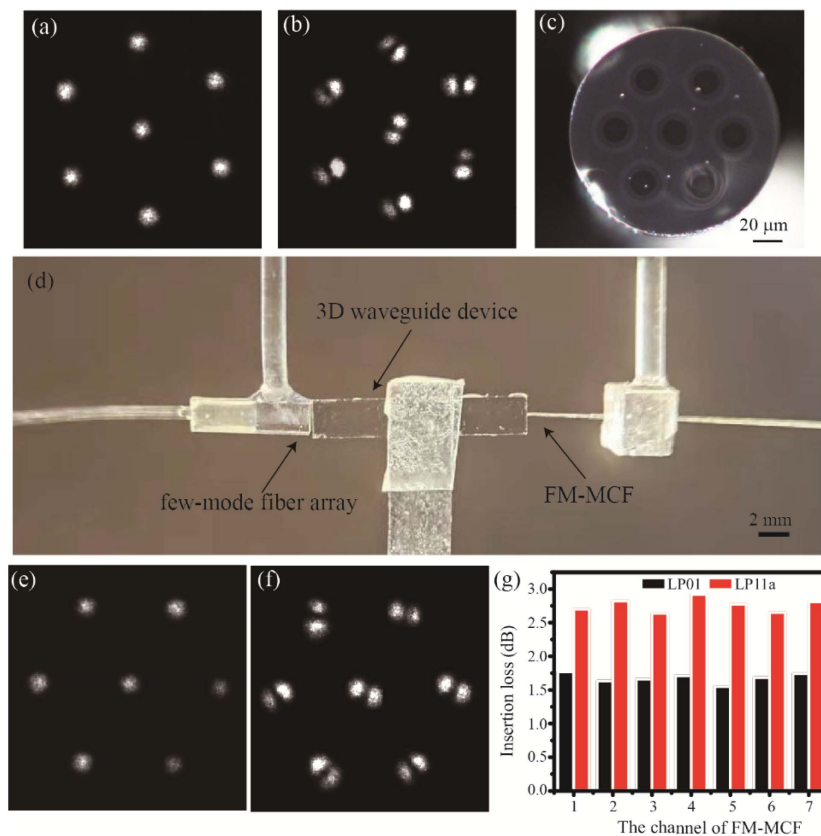

Fig. 3. Experimental intensity profiles of the (a) LP01 mode and (b) LP11a mode outputs from the 3D waveguide device. (c) Few-mode seven-core fiber. (d) Experimental setup of the few-mode fiber array coupled to an FM-MCF. Experimental intensity profiles of the (e) LP01 mode and (f) LP11a mode outputs from the few-mode seven-core fiber. (g) LP01 and LP11a modes insertion losses from the few-mode fiber array to the few-mode seven-core fiber.

and LP11a modes can be further reduced by optimizing the coupling of the fiber end waveguide face. Also, in order to balance the loss, the waveguide geometry should match better with the higher-order modes profile in the future design.

As the beam propagates in the 3D waveguide device or FM-MCF, the beam leaks, and the leaked beam causes cross talk in different waveguides or the fiber core. Therefore, we measured the cross talk of LP01, LP11a, and LP11b modes propagating in the waveguide and few-mode seven-core fiber. Figures 4(a), 4(b), and 4(c) show the cross talks of the LP01, LP11a, and LP11b modes propagating in the 3D waveguide, respectively. The different waveguide cross talk of the LP01, LP11a, and LP11b modes are less than −36 dB. This low cross talk between waveguides shows the high performance of the 3D waveguide device. The cross talk of the LP11a and LP11b modes is less than that of the LP01 mode, which is attributed to the waveguide optimization for LP11a and LP11b modes during the device fabrication. The LP01, LP11a, and LP11b mode outputs from the waveguide device are coupled to the few-mode seven-core fiber, and then we measured the cross talk between the different fiber cores. Figures 4(d), 4(e), and 4(f) show the cross talk of LP01, LP11a, and LP11b modes propagating in a 1-km few-mode seven-core fiber. The cross talk in Figs. 4(d), 4(e), and 4(f) is greater than that in Figs. 4(a), 4(b), and 4(c) because the coupling of the few-mode fiber to the few-mode seven-core fiber needs to pass through the 3D waveguide device, and the cross talk of the few-mode seven-core fiber increases with increasing fiber length. The cross talk of the few-mode seven-core fiber varies with fiber perturbation and bending. When the beam is output from a 1-km few-mode seven-core fiber, we use off-axis holography to measure the mode cross talk [19–21], and the mode cross talk between LP01 and LP11a modes is less than −20 dB. In the optical

communication experiments, due to the relatively large mode cross talk between the LP11a and LP11b generated modes, three LP mode channels cannot simultaneously transmit for 1-km long few-mode multi-core fiber in an MIMO free optical communication system. Therefore, we only demonstrate LP01 and LP11a modes multiplexing communication.

In communication experiments, we demonstrated four-channel multiplexed communication with two LP modes and two cores in a 1-km few-mode seven-core fiber via a 3D waveguide device. Figure 5(a) shows the experimental setup with four Gaussian beams output from four commercial optical modules, with each channel carrying a 10-Gbit/s on–off keying (OOK) signal. Four Gaussian beams carrying OOK signals are input from single-mode fibers to two MPLC systems [21]. Each MPLC system converts two of the four Gaussian modes into an LP01 and an LP11a modes for coaxial transmission in few-mode fibers. Two few-mode fibers form a few-mode fiber array and are simultaneously coupled to the 3D waveguide device. Two few-mode fibers correspond to two respective waveguides and are coupled to the two fiber cores of the few-mode seven-core fiber. Two light beams are transmitted in a 1-km few-mode seven-core fiber and coupled to the two few-mode fibers by another 3D waveguide device. Two few-mode fibers are respectively input to two MPLC systems. Each MPLC system converts the LP01 and LP11a modes in the few-mode fibers into two Gaussian beams at different positions, which are coupled to the single-mode fibers for error detection. In experiments, we demonstrated three groups of bit error detections for different fiber core combinations to determine the effects of different degrees of bending of the waveguide and different fiber core positions on the BER. The three FM-MCF core combinations are 3 and 4, 3 and 6, 1 and 5, and the fiber core numbers are marked as shown in Fig. 2(c). The power penalties
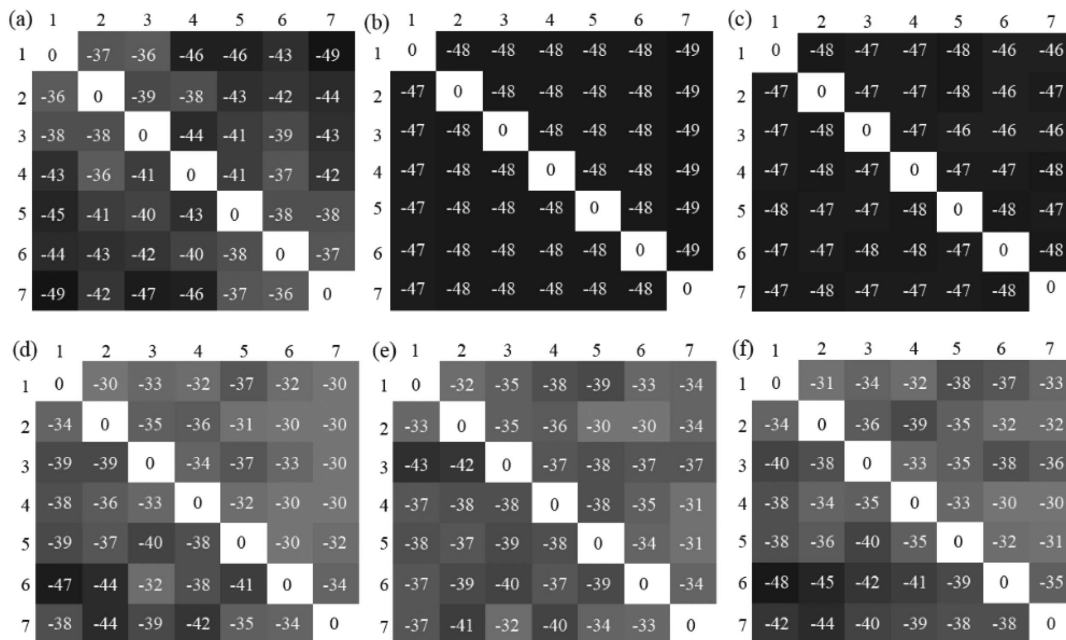

Fig. 4. Measured cross talk between different waveguides when the (a) LP01 mode, (b) LP11a mode, and (c) LP11b mode propagate in the waveguide. Measured cross talk between different fiber cores when the (d) LP01 mode, (e) LP11a mode, and (f) LP11b mode propagate in the 1-km few-mode seven-core fiber.
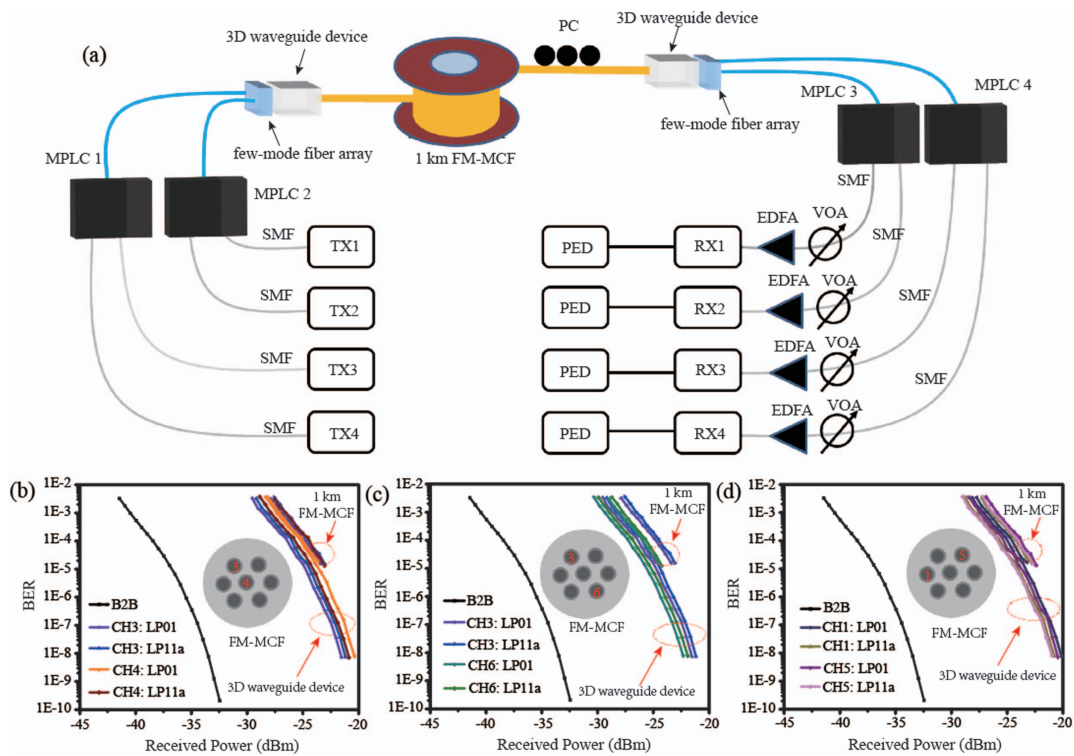
Fig. 5. (a) The setup of SDM communication system based on the few-mode seven-core fiber; TX, transmitter; SMF, single-mode fiber; PC, polarization controller; VOA, variable optical attenuator; EDFA, erbium-doped fiber amplifier; RX, receiver, PED, programmable error detector. Bit error rate (BER) curves of (b) cores 3 and 4, (c) cores 3 and 6, (d) cores 1 and 5.
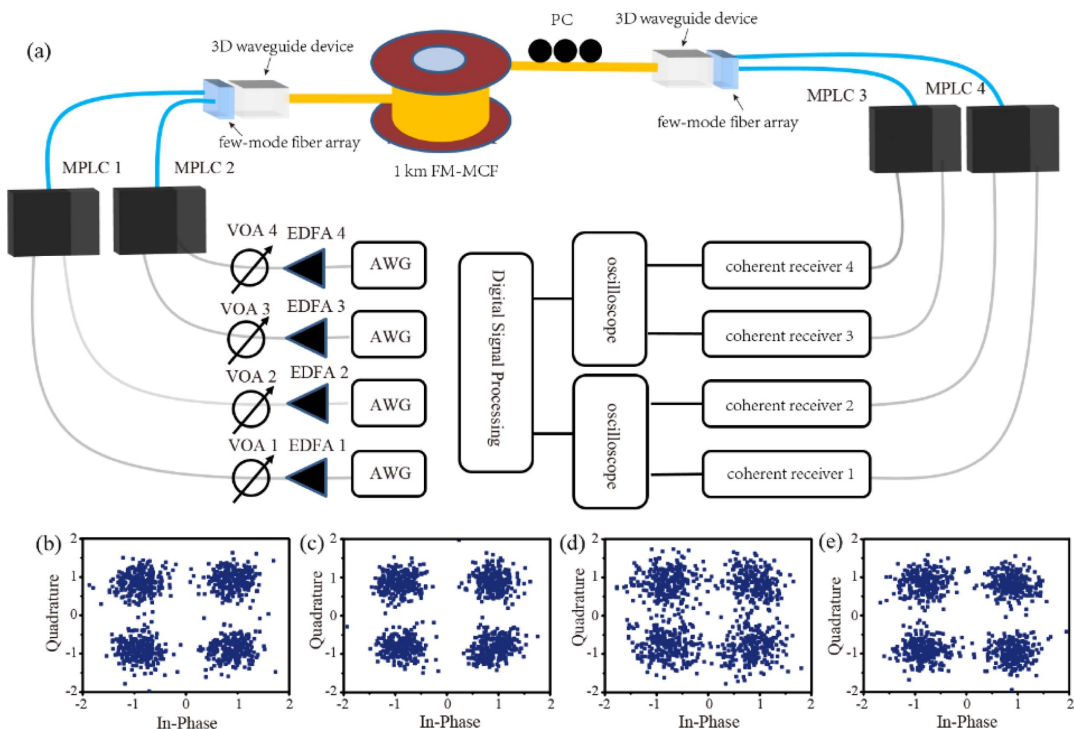

Fig. 6. (a) The setup of SDM QPSK communication system based on the few-mode seven-core fiber. Constellations of the QPSK signals: (b) with fiber cores 3 of LP11a mode; (c) with fiber cores 3 of LP01 mode; (d) with fiber cores 4 of LP11a mode; (e) with fiber cores 4 of LP01 mode.

of the three groups of BER curves in Figs. 5(b)–5(d) are all less than 13 dB, including the MPLC system, 3D waveguide device, and FM-MCF. The power penalty of Figs. 5(b) and 5(c) is about 1 dB less than that of Fig. 5(d), which is attributed to the larger waveguide bending in channels 1 and 5. The insertion loss between the FM-MCF and 3D waveguide device is 3 dB, resulting in a shorter BER curve and larger power penalty for the 1-km FM-MCF. For visualization purposes, we also measured the constellations of the four channels carrying 10-Gbit/s QPSK signals consisting of two LP modes and two cores, the setup as shown in Figs. 6(a). Figures 6(b)–6(e) show the constellations with the fiber cores 3 of LP11a mode, the fiber cores 3 of LP01 mode, the fiber cores 4 of LP11a mode, and the fiber cores 4 of LP01 mode, respectively. We can see that there is some overlap in the constellations, which can be corrected by the algorithm. These communication experiments demonstrate that the 3D waveguide device provides a solution for FM-MCF coupling, and SDM based on the 3D waveguide device and the FM-MCF can greatly improve fiber capacity. Theoretically, each core of a few-mode seven-core fiber transmits two LP modes, which can increase the capacity by a factor of 14 compared with a single-mode fiber. In follow-up research, the FM-MCF capacity can be further improved by improving the waveguide fabrication process to enable the 3D waveguide device to support higher-order LP modes transmission.

4. CONCLUSION

In conclusion, we proposed and demonstrated a 3D waveguide device for few-mode multi-core fiber optical communications. The 3D waveguide device was fabricated by femtosecond laser direct writing, and supports LP01, LP11a, and LP11b modes transmission. We optimized the waveguide bending to reduce mode leakage and cross talk. The 3D waveguide device coupled multiple groups of LP01 and LP11a modes into a 1-km few-mode seven-core fiber with an insertion loss of less than 3 dB. In communication experiments, we demonstrated four-channel multiplexing communication in a few-mode seven-core fiber consisting of two LP modes and any two fiber cores. Theoretically, 14-channel multiplexing communication is possible with a 3D waveguide device and a few-mode seven-core fiber. The FM-MCF capacity can be further improved by increasing the number of channels in the FM-MCF, which mainly involves increasing the number of channels in the

3D waveguide device. The number of channels in the 3D waveguide device can be increased by increasing the waveguide diameter or the effective refractive index difference between the waveguide and surroundings. Numerical simulations show that when the refractive index difference is 0.004 and the waveguide diameter is 17.5 μm, the waveguide supports transmission up to the LP21 mode. When the waveguide diameter is 16.5 μm, we can increase the refractive index difference between the waveguide and the cladding to support the transmission of higher-order LP modes by increasing the repetition rate and pulse width of the femtosecond laser or changing the substrate. Improvements in waveguide fabrication processes can enable 3D waveguide devices to support higher-order LP-modes transmission and further increase FM-MCF capacity. SDM consisting of 3D waveguide devices and FM-MCFs is expected to realize ultra-high-capacity multiplexed communication.

APPENDIX A: FEMTOSECOND LASER DIRECT WRITING TO FABRICATE 3D WAVEGUIDE DEVICE

Figure 7 is the setup of the 3D waveguide device fabricated by femtosecond laser direct writing. The femtosecond beam with a wavelength of 1030 nm, a pulse width of 180 fs, and a repetition rate of 200 kHz is output from the laser, and the beam size is adjusted by the 4f system. The femtosecond beam is filtered by aperture diaphragm and filter to filter stray light, and the femtosecond beam is observed by beam splitter (BS) and CCD. The femtosecond beam is focused inside the glass substrate (Corning Eagle-XG) by a 40× objective. The 3D waveguide devices are fabricated by controlling the translation stage to move the sample along the designed path. Device fabrication is optimized by adjusting various process parameters such as repetition rate, pulse width, material properties, and depth of focus.

APPENDIX B: FEW-MODE SEVEN-CORE FIBER

We use the step-index FM-MCF for LP modes transmission with a core radius of 8.25 μm. Figure 8(a) shows the effective refractive index difference radius of a fiber core in FM-MCF. The numerical simulation of FM-MCF by COMSOL shows that FM-MCF supports LP01, LP11a or LP11b, LP21a or
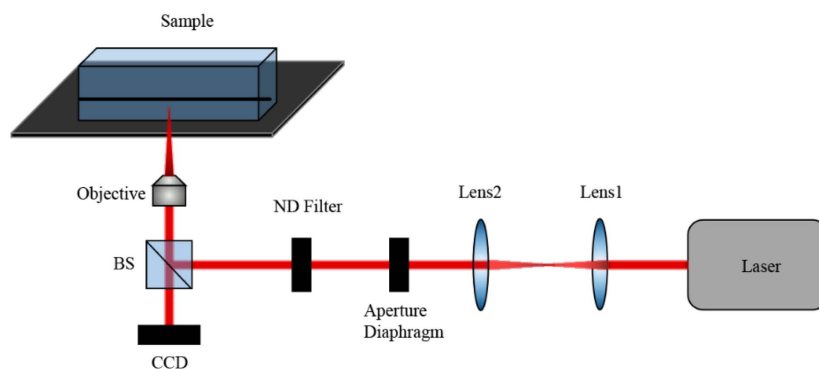

Fig. 7. Fabrication setup for 3D waveguide devices based on femtosecond laser direct writing.
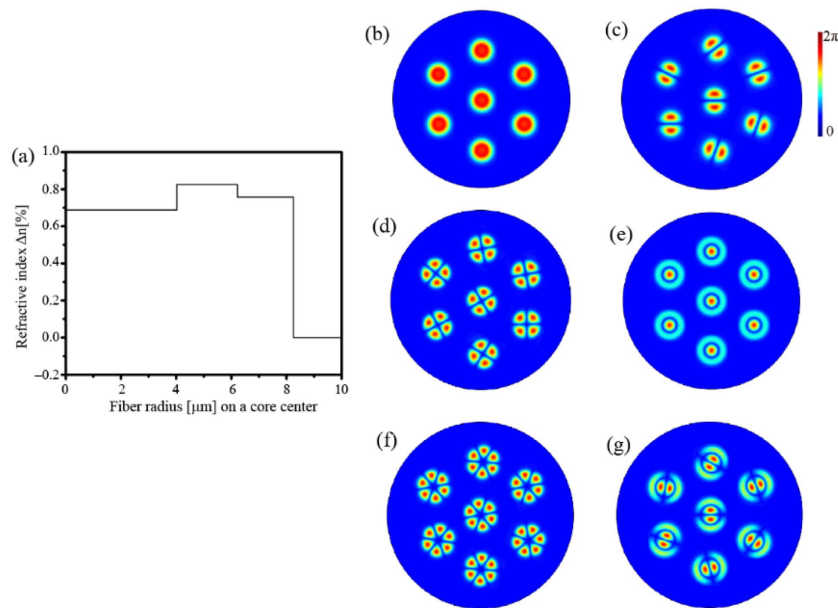
Fig. 8. (a) The effective refractive index difference versus radius of a fiber core in FM-MCF. Numerical simulation calculations show that the FM-MCF supports (b) LP01, (c) LP11a or LP11b, (d) LP21a or LP21b, (e) LP02, (f) LP31a or LP31b, (g) LP12a or LP12b modes transmission.

LP21b, LP02, LP31a or LP31b, LP12a or LP12b modes transmission, as shown in Figs. 8(b)–8(g).

Disclosures. The authors declare no conflicts of interest.

Data Availability. Data underlying the results presented in this paper are not publicly available at this time but may be obtained from the authors upon reasonable request.

†These authors contributed equally to this paper.

REFERENCES

1. R.-J. Essiambre and R. W. Tkach, "Capacity trends and limits of optical communication networks," Proc. IEEE **100**, 1035–1055 (2012).
2. R. S. Romaniuk, "Multicore optical fibers," Rev. Roum. Phys. **32**, 99–112 (1987).
3. K. Saitoh and S. Matsuo, "Multicore fiber technology," J. Lightwave Technol. **34**, 55–66 (2016).
4. S. Berdague and P. Facq, "Mode division multiplexing in optical fibers," Appl. Opt. **21**, 1950–1955 (1982).
5. N. Bozinovic, Y. Yue, Y. Ren, M. Tur, P. Kristensen, H. Huang, A. E. Willner, and S. Ramachandran, "Terabit-scale orbital angular momentum mode division multiplexing in fibers," Science **340**, 1545–1548 (2013).
6. G. Li, N. Bai, N. Zhao, and C. Xia, "Space-division multiplexing: the next frontier in optical communication," Adv. Opt. Photonics **6**, 413–487 (2014).
7. D. J. Richardson, J. M. Fini, and L. E. Nelson, "Space-division multiplexing in optical fibres," Nat. Photonics **7**, 354–362 (2013).
8. B. J. Puttnam, G. Rademacher, and R. S. Luís, "Space-division multiplexing for optical fiber communications," Optica **8**, 1186–1203 (2021).
9. P. Sillard, M. Bigot-Astruc, and D. Molin, "Few-mode fibers for mode-division-multiplexed systems," J. Lightwave Technol. **32**, 2824–2829 (2014).
10. A. Li, X. Chen, A. Al Amin, J. Ye, and W. Shieh, "Space-division multiplexed high-speed superchannel transmission over few-mode fiber," J. Lightwave Technol. **30**, 3953–3964 (2012).
11. L. Allen, M. W. Beijersbergen, R. J. C. Spreeuw, and J. P. Woerdman, "Orbital angular-momentum of light and the transformation of Laguerre-Gaussian laser modes," Phys. Rev. A **45**, 8185–8189 (1992).
12. J. Wang, J.-Y. Yang, I. M. Fazal, N. Ahmed, Y. Yan, H. Huang, Y. Ren, Y. Yue, S. Dolinar, M. Tur, and A. E. Willner, "Terabit free-space data transmission employing orbital angular momentum multiplexing," Nat. Photonics **6**, 488–496 (2012).
13. J. Chen, C. Wan, and Q. Zhan, "Engineering photonic angular momentum with structured light: a review," Adv. Photonics **3**, 064001 (2021).
14. B. Ndagano, H. Sroor, M. McLaren, C. Rosales-Guzman, and A. Forbes, "Beam quality measure for vector beams," Opt. Lett. **41**, 3407–3410 (2016).
15. J. Fang, Z. Xie, T. Lei, C. Min, L. Du, Z. Li, and X. Yuan, "Spin-dependent optical geometric transformation for cylindrical vector beam multiplexing communication," ACS Photonics **5**, 3478–3484 (2018).
16. G. C. G. Berkhout, M. P. J. Lavery, J. Courtial, M. W. Beijersbergen, and M. J. Padgett, "Efficient sorting of orbital angular momentum states of light," Phys. Rev. Lett. **105**, 153601 (2010).

17. Y. H. Wen, I. Chremmos, Y. J. Chen, Y. F. Zhang, and S. Y. Yu, "Arbitrary multiplication and division of the orbital angular momentum of light," Phys. Rev. Lett. **124**, 213901 (2020).

18. G. Ruffato, M. Massari, G. Parisi, and F. Romanato, "Test of mode-division multiplexing and demultiplexing in free-space with diffractive transformation optics," Opt. Express **25**, 7859–7868 (2017).

19. G. Labroille, B. Denolle, P. Jian, P. Genevaux, N. Treps, and J.-F. Morizur, "Efficient and mode selective spatial mode multiplexer based on multi-plane light conversion," Opt. Express **22**, 15599–15607 (2014).

20. N. K. Fontaine, R. Ryf, H. Chen, D. T. Neilson, K. Kim, and J. Carpenter, "Laguerre-Gaussian mode sorter," Nat. Commun. **10**, 26 (2019).

21. J. Fang, J. Bu, J. Li, C. Lin, A. Kong, X. Yin, H. Luo, X. Song, Z. Xie, T. Lei, and X. Yuan, "Performance optimization of multi-plane light conversion (MPLC) mode multiplexer by error tolerance analysis," Opt. Express **29**, 37852–37861 (2021).

22. G. Ruffato, V. Grillo, and F. Romanato, "Multipole-phase division multiplexing," Opt. Express **29**, 38095–38108 (2021).

23. S. Matsuo, K. Takenaga, Y. Sasaki, Y. Amma, S. Saito, K. Saitoh, T. Matsui, K. Nakajima, T. Mizuno, H. Takara, Y. Miyamoto, and T. Morioka, "High-spatial-multiplicity multicore fibers for future dense space-division-multiplexing systems," J. Lightwave Technol. **34**, 1464–1475 (2016).

24. S. Beppu, K. Igarashi, M. Kikuta, D. Soma, T. Nagai, Y. Saito, H. Takahashi, T. Tsuritani, I. Morita, and M. Suzuki, "Weakly coupled 10-mode-division multiplexed transmission over 48-km few-mode fibers with real-time coherent MIMO receivers," Opt. Express **28**, 19655–19668 (2020).

25. D. Soma, S. Beppu, Y. Wakayama, K. Igarashi, T. Tsuritani, I. Morita, and M. Suzuki, "257-Tbit/s weakly coupled 10-mode C + L-band WDM transmission," J. Lightwave Technol. **36**, 1375–1381 (2018).

26. J. Sakaguchi, W. Klaus, Y. Awaji, N. Wada, T. Hayashi, T. Nagashima, T. Nakanishi, T. Taru, T. Takahata, and T. Kobayashi, "228-spatial-channel bi-directional data communication system enabled by 39-core 3-mode fiber," J. Lightwave Technol. **37**, 1756–1763 (2019).

27. J. Zhang, G. Zhu, J. Liu, X. Wu, J. Zhu, C. Du, W. Luo, Y. Chen, and S. Yu, "Orbital-angular-momentum mode-group multiplexed transmission over a graded-index ring-core fiber based on receive diversity and maximal ratio combining," Opt. Express **26**, 4243–4257 (2018).

28. F. Z. Tan, W. M. Lyu, S. Y. Chen, Z. Y. Liu, and C. Y. Yu, "Contactless vital signs monitoring based on few-mode and multi-core fibers," Opto-Electron. Adv. **3**, 190034 (2020).

29. G. Rademacher, B. J. Puttnam, R. S. Luis, J. Sakaguchi, W. Klaus, T. A. Eriksson, Y. Awaji, T. Hayashi, T. Nagashima, T. Nakanishi, T. Taru, T. Takahata, T. Kobayashi, H. Furukawa, and N. Wada, "Highly spectral efficient C plus L-band transmission over a 38-core-3-mode fiber," J. Lightwave Technol. **39**, 1048–1055 (2021).

30. D. Soma, Y. Wakayama, S. Beppu, S. Sumita, T. Tsuritani, T. Hayashi, T. Nagashima, M. Suzuki, M. Yoshida, K. Kasai, M. Nakazawa, H. Takahashi, K. Igarashi, I. Morita, and M. Suzuki, "10.16-peta-b/s dense SDM/WDM transmission over 6-mode 19-core

fiber across the C plus L band," J. Lightwave Technol. **36**, 1368–1375 (2018).

31. W. Klaus, J. Sakaguchi, B. J. Puttnam, Y. Awaji, N. Wada, T. Kobayashi, and M. Watanabe, "Free-space coupling optics for multi-core fibers," IEEE Photonics Technol. Lett. **24**, 1902–1905 (2012).

32. N. Lindenmann, S. Dottermusch, M. L. Goedecke, T. Hoose, M. R. Billah, T. P. Onanuga, A. Hofmann, W. Freude, and C. Koos, "Connecting silicon photonic circuits to multicore fibers by photonic wire bonding," J. Lightwave Technol. **33**, 755–760 (2015).

33. V. I. Kopp, J. Park, J. Singer, D. Neugroschl, and A. Gillooly, "Low return loss multicore fiber-fanout assembly for SDM and sensing applications," in Optical Fiber Communication Conference (OFC) (2020), paper M2C.3.

34. N. Riesen, S. Gross, J. D. Love, Y. Sasaki, and M. J. Withford, "Monolithic mode-selective few-mode multicore fiber multiplexers," Sci. Rep. **7**, 6971 (2017).

35. Q. Huang, Y. Wu, W. Jin, and K. S. Chiang, "Mode multiplexer with cascaded vertical asymmetric waveguide directional couplers," J. Lightwave Technol. **36**, 2903–2911 (2018).

36. H. Chen, N. K. Fontaine, R. Ryf, B. Guan, S. J. Ben Yoo, and T. Koonen, "Design constraints of photonic-lantern spatial multiplexer based on laser-inscribed 3-D waveguide technology," J. Lightwave Technol. **33**, 1147–1154 (2015).

37. Z. Xie, S. Gao, T. Lei, S. Feng, Y. Zhang, F. Li, J. Zhang, Z. Li, and X. Yuan, "Integrated (de)multiplexer for orbital angular momentum fiber communication," Photonics Res. **6**, 743–749 (2018).

38. L. W. Chen, Y. M. Yin, Y. Li, and M. H. Hong, "Multifunctional inverse sensing by spatial distribution characterization of scattering photons," Opto-Electron. Adv. **2**, 19001901 (2019).

39. X. Lu, Y. Shao, C. Zhao, S. Konijnenberg, X. Zhu, Y. Tang, Y. Cai, and H. P. Urbach, "Noniterative spatially partially coherent diffractive imaging using pinhole array mask," Adv. Photon. **1**, 016005 (2019).

40. C. Jin, M. Afsharnia, R. Berlich, S. Fasold, C. Zou, D. Arslan, I. Staude, T. Pertsch, and F. Setzpfandt, "Dielectric metasurfaces for distance measurements and three-dimensional imaging," Adv. Photonics **1**, 036001 (2019).

41. X. Chen, Z. Fu, Q. Gong, and J. Wang, "Quantum entanglement on photonic chips: a review," Adv. Photonics **3**, 064002 (2021).

42. D. Tan, Z. Wang, B. Xu, and J. Qiu, "Photonic circuits written by femtosecond laser in glass: improved fabrication and recent progress in photonic devices," Adv. Photonics **3**, 024002 (2021).

43. D. Z. Tan, B. Zhang, and J. R. Qiu, "Ultrafast laser direct writing in glass: thermal accumulation engineering and applications," Laser Photonics Rev. **15**, 2000455 (2021).

44. Y. C. Jia, S. X. Wang, and F. Chen, "Femtosecond laser direct writing of flexibly configured waveguide geometries in optical crystals: fabrication and application," Opto-Electron. Adv. **3**, 190042 (2020).

45. F. J. Mustieles, E. Ballesteros, and P. Baquero, "Theoretical S-bend profile for optimization of optical wave-guide radiation losses," IEEE Photonics Technol. Lett. **5**, 551–553 (1993).

46. V. Kumar and V. Priye, "3-D multilayer S-bend silicon waveguide optical interconnect," IEEE Photonics Technol. Lett. **30**, 1040–1043 (2018).